Chapter 7

Circle Maps

7.1 A New Global Topology

The global topology of phase space can have dramatic consequences: A period-3 orbit forces orbits of every period if it belongs to a map of an interval into itself, none if the state space is two-dimensional or is the unit circle. This indicates that qualitatively different behaviors can appear when phase space topology is changed. Accordingly, this section is devoted to a brief review of dynamical properties of maps from the unit circle S^1 into itself. If S^1 is parameterized with an angular variable $\theta \in [0, 1]$, these maps can be written as $\theta_{n+1} = f(\theta_n) \pmod 1$.

Physically, the study of circle maps is motivated by the problem of coupled oscillators. Assume that we have two systems oscillating on periodic cycles at frequencies ν and ν', respectively. The state of each oscillator can be described by an angular variable $\theta(t) = \nu t \pmod 1$. In the spirit of Poincaré sections, let us sample these angles stroboscopically at the frequency ν' so that we need only measure the successive samples $\theta_n = \theta(t_0 + n/\nu')$ of the first angle, given by

$$\theta_{n+1} = (\theta_n + w) \pmod 1 \tag{7.1}$$

where $w = \nu/\nu'$. The map 7.1 describes a rotation by a fraction w of a full turn per sampling period and is denoted $R(w)$ in the following.

Two different qualitative behaviors can occur depending on the value of w. If w is a rational, p/q with $p, q \in Z$, we have that $\theta_{n+q} = \theta_n + qw \pmod 1 = \theta_n$: The dynamical regime is a periodic orbit, and θ_n takes only a finite number of different values. If w is irrational, the sequence $\{\theta_n\}$ densely fills the interval $[0, 1]$. This is a quasiperiodic regime and corresponds to the superposition of two incommensurate frequencies.

7.2 Frequency Locking and Arnol'd Tongues

It is known that the set of rational numbers is dense in $[0, 1]$ but that it has zero measure: The frequency ratio of two uncoupled oscillators is irrational with a probability of 1, even if one can find rational values arbitrarily close. However, this changes as soon as a coupling is introduced. One then observes *frequency locking*: The frequency ratio of the two oscillators remains fixed at a rational value p/q in a finite range $w \in [p/q - \Delta\rho_1, p/q + \Delta\rho_2]$.

To study this phenomenon, the following circle map was introduced by Arnol'd [**?**]:

$$\theta_{n+1} = [\theta_n + w + \frac{K}{2\pi}\sin(2\pi\theta_n)] \pmod 1 \tag{7.2}$$

which features a nonlinear coupling characterized by its strength K. Figure 7.1 displays the graph of the map obtained for $(w, K) = (0.47, 0.8)$.

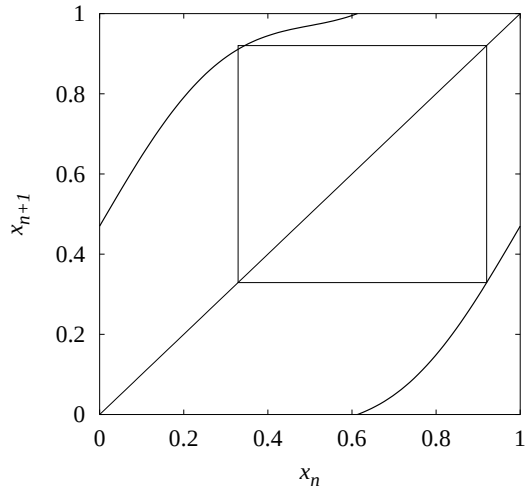

Figure 7.1: Graph of the circle map 7.2 for $w = 0.47$ and $K = 0.8$. A period-2 orbit is also represented.

To describe the asymptotic regimes of 7.2, one introduces the *rotation number* [**?**, **?**, **?**]

$$\rho = \lim_{N\to\infty} \frac{1}{N} \sum_{n=0}^{N-1} \Delta\theta_n \quad \text{with } \Delta\theta_n = [w + K/2\pi \sin(2\pi\theta_n)] \tag{7.3}$$

Note that $\rho = w$ in the limit $K = 0$. The structure of the function $\rho(w, K)$ thus provides insight into the phenomenon of frequency locking as the nonlinear coupling is increased.

When the circle map 7.2 is a homeomorphism of S^1 into itself (i.e., for $K \leq 1$), the following properties of the rotation number $\rho(w, K)$ can be established:

- The rotation number 7.3 does not depend on the orbit used to compute it.
- If $\rho(w, K)$ is irrational, the circle map is equivalent to the pure rotation $R(\rho)$; the motion is quasiperiodic.
- If $\rho(w, K) = p/q$ with p and q relatively prime integers, the asymptotic regime is a periodic orbit of period q. The periodic points of this orbit are ordered along the unit circle as with the pure rotation $R(p/q)$.

Thus, the classification of dynamical behaviors of the Arnol'd map for $K \leq 1$ amounts to determining the parameter regions in the (w, K) plane where $\rho(w, K)$ is rational.

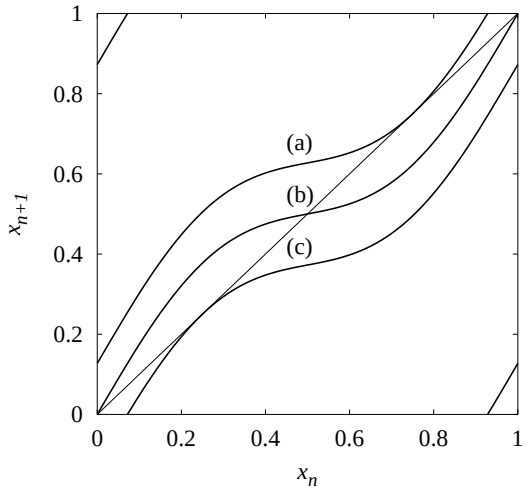

Figure 7.2: Graph of the circle map for $K = 0.8$ and (a) $w = 0.8/2\pi$; (b) $w = 0$; (c) $w = -0.8/2\pi$.

As a simple example, let us consider the region $\rho(w, K) = 0$, where the oscillator frequencies are locked to each other in a 1:1 ratio. The corresponding asymptotic regime is a fixed point $\theta_{n+1} = \theta_n$ whose location, according to 7.2, is given by the equation $w = -(K/2\pi)\sin\theta$. It is easy to see that for $w \in [-K/2\pi, +K/2\pi]$, there are two solutions, one of which is stable in the whole domain $0 \leq K \leq 1$, at least (Fig. 7.2). Indeed, the slope of the graph at the two intersections is positive (the function is monotonic) and must be lower than 1 at one of the intersections. Hence, there is a periodic orbit having multiplier $0 \leq \mu \leq 1$. For $w = \pm K/2\pi$, the graph of the map is tangent to the diagonal, indicating that the stable and unstable periodic orbits are created and destroyed through saddle-node bifurcations. Note that the width of the frequency-locking interval $\rho = 0$ increases linearly with K and corresponds at $K = 1$ to almost one-third of the possible values of w.

By determining which regions of the (w, K) plane correspond to rotation numbers $\rho(w, K) = p/q$ with a small denominator q, the diagram shown in Fig. 7.3 is obtained for $q \leq 8$. The regions of frequency locking are called *Arnol'd tongues*. Each of them corresponds to a different rational p/q, which governs the order in which they are encountered as w is increased at fixed K, since $\rho(w, K)$ is a monotonic function of w. As discussed above, tongues are bounded on both sides by saddle-node bifurcations where periodic orbits of the corresponding rotation number are created or destroyed.

It is interesting to note that the rotation numbers corresponding to the most important tongues can be classified according to a hierarchy based on an arithmetic operation on fractions. Indeed, it turns out that the principal tongue located between two tongues of rotation numbers p_1/q_1 and p_2/q_2 that satisfy $p_1q_2 - p_2q_1 = \pm 1$ is the one associated with the *Farey sum* of these two fractions, defined as follows: $p_1/q_1 \oplus p_2/q_2 = (p_1 + p_2)/(q_1 + q_2)$. Starting from the fundamental tongues 0/1 and 1/1, one first obtains the 1/2 tongue. The latter is then separated from 0/1 by 1/3 and from 1/1 by 2/3. At the third level, one obtains 1/4, 2/5, 3/5, 3/4, and so on. Tongues at a given level are wider than those at the next level, as can be checked by visual inspection of Fig. 7.3.

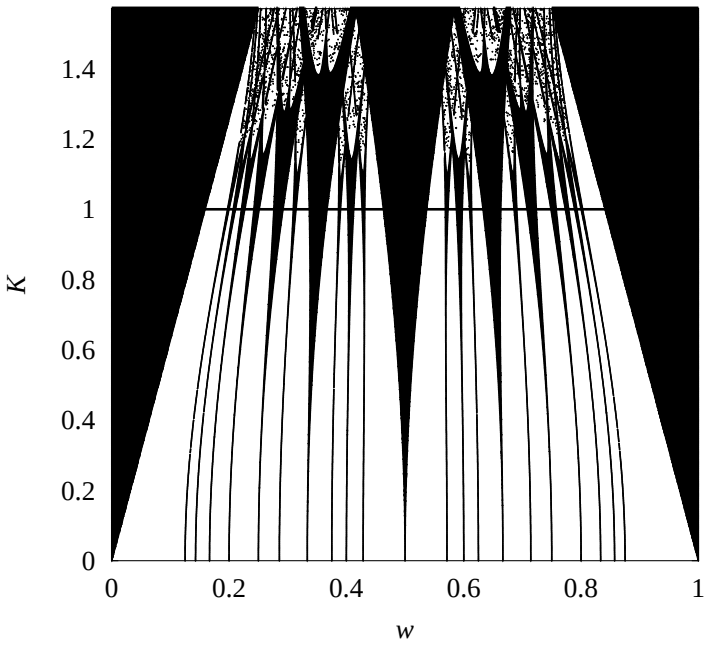

Figure 7.3: Arnol'd tongues for the circle map (7.2) corresponding to rational rotation numbers $\rho(w, K) = p/q$ with $q \leq 8$.

As K is increased from 0 to 1, the relative proportions of the quasiperiodic and periodic regimes are exchanged. At $K = 0$, quasiperiodic regimes have a probability of 1, as mentioned above. Since there are an infinite number of tongues, it might not be obvious that the total length in w of the frequency-locked intervals goes to zero as $K \to 0$. That this is the case is due to the width $\Delta w(p/q)$ of the $\rho = p/q$ tongue decreasing sufficiently fast as $K \to 0$, more precisely as $\Delta w(p/q) \sim K^q$ or $\Delta w(p/q) \sim K^{q-1}$, depending on p/q.

At $K = 1$, values of w yielding quasiperiodic regimes are confined to a Cantor set of measure 0 and of fractal dimension $D \sim 0.87$; frequency-locked regimes have measure 1. The graph of the function $\rho(w, K = 1)$, shown in Fig. 7.4, has a very peculiar structure, known as a *devil's staircase*. It is continuous and monotonic but increases only where ρ is irrational: Each rational value occurs on a finite interval. Moreover, it is self-similar: Any part of the graph contains a reduced copy of the entire graph. Incomplete devil's staircases are observed for $K < 1$ (i.e., the set of parameters yielding irrational rotation numbers then has positive measure).

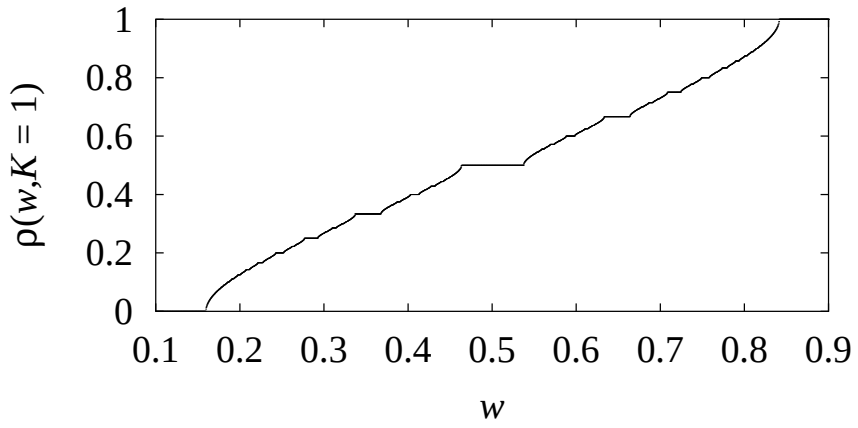

Figure 7.4: Graph of the rotation number $\rho(w, K = 1)$ is a devil's staircase.

7.3 Chaotic Circle Maps and Annulus Maps

The $K = 1$ line in the phase diagram of Fig. 7.3 is called the *critical line*. Beyond it, the circle map (7.2) has a point with zero derivative and hence is no longer invertible, which has dramatic consequences on the dynamics. On the one hand, there are no longer quasiperiodic regimes. Indeed, the latter are equivalent to a pure rotation with an irrational rotation number, which cannot be conjugate to a noninvertible map. On the other hand, more complex behavior can then appear, including chaos. Since the map (7.2) has branches with negative slope,

the stable periodic orbit can now have a negative multiplier and undergo a period doubling when the latter crosses -1. Most of the analysis carried out for the logistic map applies here: One observes cascades of period doubling leading to chaos. The white zones in the $K > 1$ part of Fig. 7.3 correspond to chaotic regimes or to periodic regimes of high period.

Another consequence of noninvertibility is that the rotation number (7.3) now depends on the initial condition. Accordingly, a given regime is characterized by a *rotation interval* $[\rho^-, \rho^+]$ rather than by a single number. This corresponds to Arnol'd tongues gradually overlapping as K is increased above 1, as can be seen in Fig. 7.3.

As discussed in the introduction to this section, invertible circle maps can be obtained rigorously as a first-return map when the dynamics is confined to a two-dimensional torus T^2. Obviously, this interpretation is not valid for noninvertible circle maps. However, exactly as the one-dimensional logistic map can be viewed as the infinitely dissipative limit of a two-dimensional horseshoe-like invertible map, noninvertible circle maps can be thought as limits of maps of an annulus into itself. Not that this interpretation is limited to circle maps having a degree of 1 (the image of the annulus winds once around the center). This is illustrated in Section 10.8 with the important example of the forced van der Pol oscillator.

7.4 van der Pol Oscillator

The van der Pol oscillator has also been studied in great detail [**?**, **?**]. The twofold symmetry complicates studies of this oscillator as well. The stretching and squeezing mechanisms responsible for creating chaotic behavior involve the twofold iteration of a basic process but a process which is different from that which operates for the Duffing oscillator. Symmetry reduction simplifies the study of this nonlinear oscillator as well. The version of the van der Pol oscillator that we study here is defined by

$$\begin{aligned} \dot{X} &= F(X,Y) &&= bY + (c - dY^2)X \\ \dot{Y} &= G(X,Y) &&= -X + A\sin(\omega t) \end{aligned}$$

In Fig. 7.5 we show a series of Poincaré sections in the X–Y space for a strange attractor generated by the van der Pol equations. Alongside each section for the original attractor, we exhibit a section in the u–v space for the attractor which has had the symmetry removed. The reduction of the period from T in the original equations with symmetry to $\frac{1}{2}T$ in the image equations is evident.

Van der Pol dynamics differs in a fundamental way from Duffing dynamics. In the latter case the stretch-and-squeeze mechanism is similar to a mapping of the interval onto itself—in fact, it is equivalent to a mapping of a (long, thin) rectangle into itself. In the case of van der Pol dynamics, the stretch-and-squeeze mechanism is similar to a mapping of the circle onto itself—in fact, it is equivalent to a mapping of an annulus into itself [**?**]. By following the stretching of the attractor around one period [$\frac{1}{2}T$; Fig. 7.6(a)], it is possible to construct

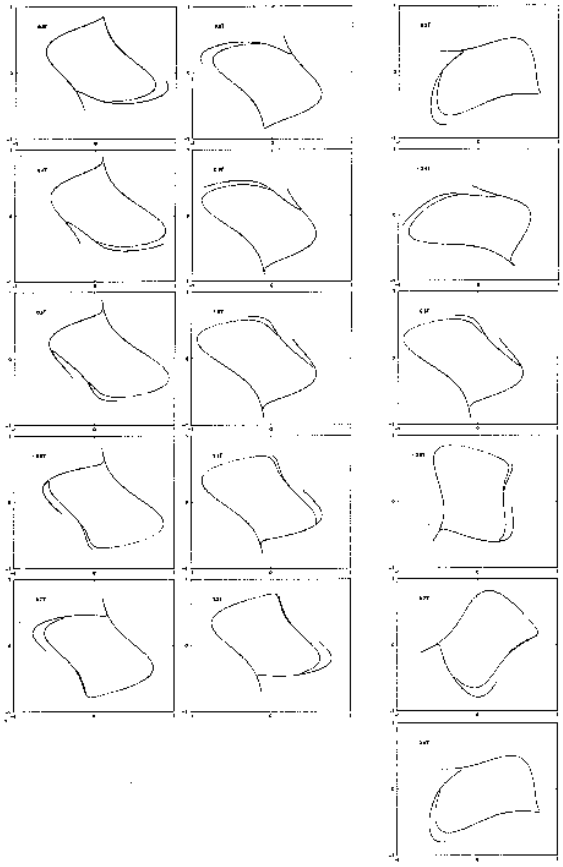

Figure 7.5: Left: Series of 10 Poincaré sections for the van der Pol attractor. The sections are spaced at $0.1T$. The symmetry $(X, Y, t) \to (-X, -Y, t + \frac{1}{2}T)$ is evident. Right: The $2 \to 1$ images of these 10 sections are shown after the symmetry has been modded out. The reduced dynamical system has period $\frac{1}{2}T$. Parameter values: $b = 0.7$, $c = 1$, $d = 10$, $A = 0.25$, $\omega = \pi/2$.

a rough approximation to a return map of the circle to itself. The return map is shown in Fig. 7.6(b). Finally, the original circle can be blown up in the transverse direction and the return map used to construct a map of the annulus to itself. This map is shown in Fig. 7.6(c).

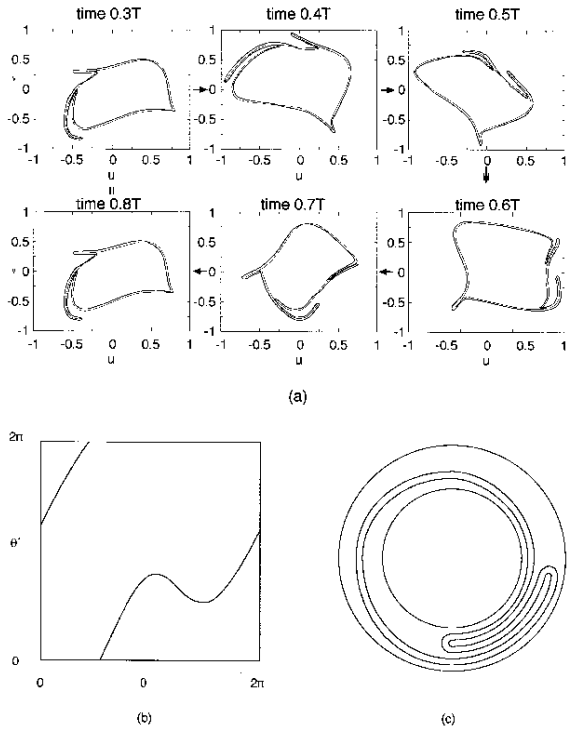

Figure 7.6: (a) By following the stretching of the attractor through a full period (here $\frac{1}{2}T$), it is possible to determine how a topological circle is mapped to itself under the symmetry reduced flow. (b) This provides a reasonable estimate for the return map. The return map for the system with full symmetry is the second iterate of this return map. (c) The return map of the circle can be blown up to provide a mapping of the annulus back to itself.

The branched manifold for the original van der Pol oscillator (at appropriate parameter values) is shown at the top of Fig. 10.14. In this representation, the left- and right-hand edges of the branched manifold must be identified, using periodic boundary conditions. The processes that take place in the first half period, from $t = 0$ to $t = \frac{1}{2}T$, are repeated in the second half period, phase-shifted by π radians. The phase shift is equivalent to the map $(X, Y) \to (-X, -Y)$. When the symmetry is removed (Fig. 7.7, bottom), the stretching and squeezing that takes place during the first half period is extended a further

π radians. As a result, the stretching and squeezing that takes place during the second half period repeats that of the first half period. The period of the flow has been reduced to $\frac{1}{2}T$. The simplified branched manifold (bottom) shows three branches, compared to the six of the original branched manifold.

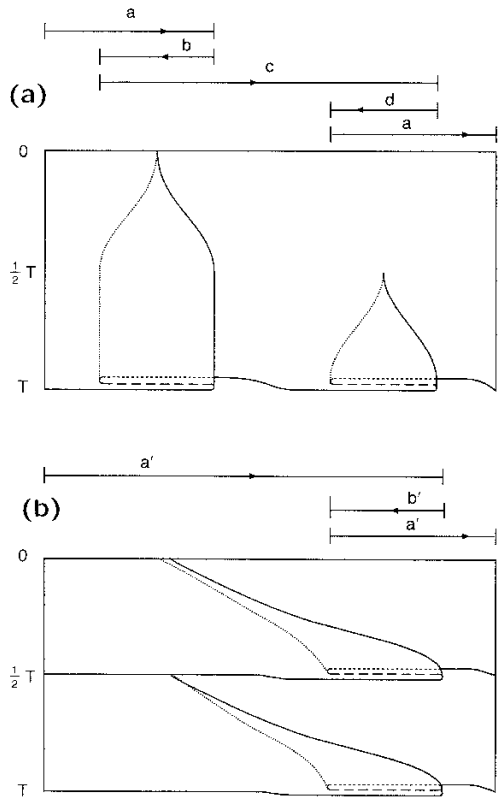

Figure 7.7: (a) The stretching and squeezing that take place for the van der Pol oscillator are represented by this template with six branches. The left- and right-hand edges are to be identified. (b) After the inversion symmetry has been removed, the stretching and folding is represented by this branched manifold. The basic periodicity has been reduced from T to $\frac{1}{2}T$.

The perestroika of the van der Pol equations is governed by the same constraints as that of the Duffing equations. It is only the topology that is different. Specifically:

- As the ratio T/T_r increases, the global torsion of the branches present in the branched manifold describing the strange attractor increases systematically.

- As the strength of the nonlinear coupling increases, the average number of branches required to describe the strange attractor increases.

The details are summarized in Fig. 7.8. In Fig. 7.8(a) we present a return map of the circle to itself: $\theta \to \theta'$. In this map we take $0 \leq \theta \leq 2\pi$, with 0 and 2π identified. We should do the same for the image θ', but do not, to make the argument clearer. In this figure, the circumference of the circle is stretched by a factor of approximately 3, with $0 \to 0$. The period-1 orbits are identified by the intersections of the return map with the diagonals. The branches of the return map are dressed by their local torsion. There are four fixed points when we identify the points at 0 and 2π. The nonlinearity governs the amplitude of the return map (approximately 4π) and the ratio T/T_r governs the "rotation" (here 0). As T/T_r increases, the return map is rigidly shifted upward.

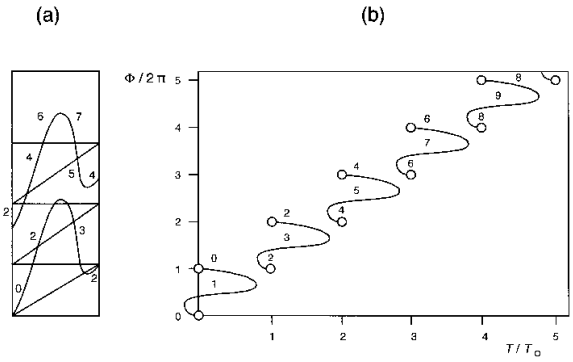

Figure 7.8: (a) A return map $\theta \to \theta' = f(\theta)$ of the circle to itself has amplitude governed by the strength of the nonlinearity and rotation (vertical displacement) governed by the ratio of time scales: T/T_r. The branches of the map are dressed by the local torsion of the corresponding period-1 orbit in the flow. The image θ' has not been taken mod 2π for the sake of clarity. (b) The period-1 orbits that exist for any value of T/T_r are indicated in this circle map analog of a snake diagram. Each sinuous curve is a "bubble," difficult to recognize because of the 2π vertical boundary conditions. Unlike the snake, the period-1 orbits mutually create and annihilate.

The evolution of the period-1 orbits as a function of increasing T/T_r is summarized in Fig. 7.8(b). As T/T_r increases above 0, the period-1 orbit at $0 = 2\pi$ and the one near 2π with torsion 2 collide and annihilate in an inverse saddle-node bifurcation. The two fixed points on branches 2 and 3 separate, and by the time $f(0) = 2\pi$, the entire curve has been shifted up by 2π. The return map has been shown for the case $f(0) \simeq 3\pi$ in Fig. 10.15(a). In this case the orientation-preserving branches have torsions 2, 4, and 6, while the orientation-reversing branches have torsions 7 and 5. Figure 10.15(b) for the

circle map is the analog of the snake diagram (Fig. 10.11) for the scroll return map of the interval to itself. It consists of a sequence of "bubbles" which do not look like bubbles. For example, the bubble at $T/T_r = 2$ consists of two period-1 orbits with torsions 4 and 5. These orbits are created in a saddle-node bifurcation for $T/T_r \sim \frac{7}{4}\pi$ and annihilate in an inverse saddle-node bifurcation for $T/T_r \sim \frac{11}{4}\pi$. For any value of T/T_r there is only an even number of period-1 orbits. This is in opposition to the Duffing case, in which the snake diagram indicates that only an odd number of period-1 orbits is present for any value of T/T_r. The difference, even (for maps of S^1) or odd (for maps of R^1), is tied intimately to the global topology of a one-dimensional surface. This surface is the intersection of the branched manifold for a strange attractor with a Poincaré section.

7.5 Summary

Although maps are very simple dynamical systems, they display most of the key features of chaos. This has allowed us to become familiar with concepts that will appear throughout this book, without excessive mathematical difficulty.

Even the simplest dynamical system that one can think of, the logistic map, is able to reproduce surprisingly well qualitative behaviors that are observed experimentally in the laser system described in Chapter 1. As a control parameter is varied, it experiences bifurcations, in particular a period-doubling cascade leading to chaos, and a variety of chaotic regimes.

The simple structure of the logistic map makes it possible to study one of the basic mechanisms responsible for chaotic behavior, namely stretching. In its most chaotic regime, the logistic map is basically a "multiply by two" machine. This has far-reaching consequences: Sensitivity to initial conditions, existence of an infinite number of periodic orbits which are dense in the invariant set, and so on.

Stretching is at the root of an extremely powerful tool for unfolding chaos, symbolic dynamics. Thanks to the unlimited magnification provided by sensitivity to initial conditions, a series of coarse-grained measurements of the system state suffice to specify it with arbitrary accuracy. Symbolic dynamics not only allows us to classify orbits (e.g., how many periodic orbits of period p?) but also to study their genealogies (e.g., in which order do orbits appear? Which orbit is a period-doubled orbit from another?). By studying the grammar of a chaotic system, we can classify regimes and compute quantitative invariants such as topological entropy. Not all of the results obtained (e.g., the universal sequence) can be directly extended to higher dimensions. That there are topological invariants (e.g., permutations) that both are deeply related to symbolic dynamics and play a major role in forcing relations will later prove to be a key property.

The logistic map is a noninvertible system. Many physical systems are described by ODEs and thus are associated with invertible maps, such as the Hénon map. A chaotic invertible map shares many properties with noninvert-

ible ones. In particular, the dynamics in the unstable space is associated with a noninvertible map, as the example of the horseshoe map shows. There are also new problems, such as constructing relevant symbolic encodings in that case. Finally, global phase space topology can have a deep influence of phenomena observed, as exemplified by circle maps.